Quasi-static behaviour of crash components with steel skins and polymer foam cores

Aase Reyes[a,b,*] and Tore Børvik[a,b]

[a] *Structural Impact Laboratory (SIMLab), Department of Structural Engineering, Norwegian University of Science and Technology (NTNU), NO-7491 Trondheim, Norway*

[b] *Centre for Advanced Structural Analysis (CASA), NTNU, NO-7491 Trondheim, Norway*

Abstract

Different types of crash components are extensively used by the automotive industry to absorb energy during car accidents. Such components typically consist of sandwich structures with thin metal or composite plates as skins and a cellular foam as core to dissipate the energy. In this study, the quasi-static behaviour of two types of polymeric foams with different densities, namely extruded polystyrene (XPS) and expanded polypropylene (EPP), utilized as core material in a crash component, has been investigated. First, an extensive material test program involving compression tests on cubic specimens loaded in different material directions was carried out to reveal the mechanical properties of the foams. Second, quasi-static impact tests were conducted on various target configurations consisting of 0.8 mm thick skins of Docol 600DL steel and the various foam materials as core. In these tests, the applied force and the displacement of the striker were registered by the test machine, while digital cameras and 3D-DIC were used to measure the back-plate out-of-plane displacement of the various components. It seems clear from the presented results that if low weight combined with maximum energy absorption are the primary interests, an XPS foam as core seems to be beneficial, while if force reduction and minimum back-plate displacement are most important, an EPP foam as core seems to be a better choice. Thus, the response of the crash component is largely determined by the properties of the core material during quasi-static loading.

Keywords: Sandwich structures; XPS; EPP; Docol 600DL; Material tests; Component tests; Energy absorption

1. Introduction

Energy absorbing systems have become increasingly important in the automotive industry to ensure protection of the car body and the passengers during a crash event [1]. At the same time, research in this area is evolving by the quest for new innovative designs and new materials [2], often driven by the prospect of weight reduction. Such energy-absorbing systems include

* Corresponding author.

e-mail address: aase.reyes@ntnu.no (A. Reyes)

crash pads inside the vehicle to improve the passengers' survivability, special designs for pedestrian safety and bumper-beam systems with crash boxes for increased crashworthiness. They could also consist of a sandwich structure with a core material inserted between two skins. The core is typically a light and soft cellular material such as a foam that absorbs energy during crushing. Traditionally the sandwich structure has been used as a structural element with high specific bending stiffness and strength, where the main intention of the core is to separate and stabilize the outer sheets against buckling under edgewise compression, torsion or bending [3]. Today, foams can also be used inside other structural elements of the external body for passengers' passive safety in a car crash [4]. In some cases, foams are used to absorb energy without any outer skin or casing [5]-[6]. There are, however, many factors to consider when designing an energy absorber. The energy absorption should be as high as possible, which can be achieved through large forces and/or displacements of the component. On the other hand, the transferred loads should not be too high during a collision, both for the passenger safety and the structural integrity. Furthermore, there might be limitations on the maximum displacement of the crash component. If the load can be held constant at a sufficiently low level, while at the same time absorb a considerable amount of energy, it would be favourable.

Cellular materials such as honeycombs, open and closed cell foams, and metal hollow spheres, have excellent characteristics as potential blast and impact energy absorbers due to their ability to deform uniformly over a long stroke at an almost constant load [7]. The properties of these materials are governed by the topology of the cell structure and the intrinsic properties of the cell-wall material (often denoted the constituent or base material), where the topology defines how the constituent material is packed in space to form a porous structure. While honeycombs typically have a periodic topology, the topology of foams is in general stochastic. Polymeric foams have been particularly attractive because of their low weight combined with excellent energy absorbing capability, insulation properties, easy production, low price and design flexibility. Nowadays, they have a variety of applications, such as protective materials including packaging and head protective systems, and in a multitude of aerospace, marine and automotive components [8]-[10]. A large number of polymeric foams are also available, and their microstructures depend on the base material and the production process that influence the density as well as the thermal and mechanical properties.

In general, foams are classified according to whether they have an open or closed cell structure. Despite the many variations, the typical mechanical response of most polymeric foams in compression consists of three phases of deformation, namely (1) the linear elastic response, (2) the plateau region, and (3) the densification [11]. The linear elastic response is

governed by the reversible bending or distortion of the cell walls during small deformations [12]. The plateau region with large deformations that occur at modestly increasing stress levels is primarily related to buckling of the cell walls. This is what makes foams so attractive for energy absorption: the ability to withstand large deformations at an approximately constant stress level. Densification begins when the cell walls start to interact with each other, and this causes the stress to rise rapidly. The theoretical densification strain is defined as when zero void ratio is reached [12], indicating that all cells have collapsed, but the meaning of this term varies in the literature and is often taken as the strain at the onset of the densification phase [13].

According to Gibson and Ashby [11], important properties of foams include low relative density (< 0.3) and high specific energy absorption, where the absorbed energy per unit volume is approximated by the area beneath the stress-strain curve. The mechanical properties have also been found to depend strongly on the foam density; e.g. the material's elastic modulus and plateau stress increase, while the densification strain decreases, with increasing density [11]. Because of the apparent foam density dependence, several authors have played with the idea of designing foam components with graded density according to where compressive strength is needed [14]-[15]. The constitutive behaviour of most foams is also found to be both strain-rate and temperature dependent [16]. Recently a comprehensive review on the dynamic compressive behavior of cellular materials was published by Sun and Li [17]. The overall conclusion from the reviewed studies is that polymeric foams are in general highly strain-rate sensitive.

Especially expanded polypropylene (EPP) has received a lot of attention over the years [18]-[23]. Maheo et al. [23] tested EPP foams to study the multiaxial behaviour of the material. They performed hydrostatic, shear and pressure-shear tests, and found a clear volumetric change for the foams. The compressive behaviour of extruded polystyrene (XPS) was studied by Sadek and Fouad [24]. The plates used in their work showed strong anisotropic behaviour in compressive strength. They also tried to model the microstructure using finite element simulations. Avalle et al. [4], [8] carried out a large experimental campaign on different foams, including closed-cell and open-cell structures with various densities, subjected to both quasi-static and impact loading, and used an efficiency diagram to compare the behaviour of the different foams [8]. Miltz and Ramon [25] compared the energy absorption characteristics for PUR, PE and PS foams, and found that that the stiffer PS and PE foams attain better efficiency at higher strains than the more flexible PUR foams.

A traditional sandwich panel consists of two sheets bonded to a deformable core [26]. The idea is that the core material will absorb energy during loading, and as a result, lower the forces and displacements transferred to the surrounding structure. The choice of skin and core material

is usually governed by the application. Yuen et al. [27] differs between sacrificial claddings (i.e., a sandwich panel that is fixed to an existing structure) and sandwich structures where the rear side is free to deform. As the core and sheets can consist of several different materials, there have been numerous studies on different types of sandwich structures, depending on the load case. Some examples are glass-fibre-reinforced polymer (GFRP) skins in combination with PS foams [28], PP honeycombs [28]-[29], balsa wood [28], cork [28] and PU foam [29]. Zhang et al. [30] studied the static and dynamic crushing of sandwich panels consisting of carbon-fibre-reinforced polymer (CFRP) skins filled with very different materials (EPP, aluminium honeycomb, rubber foam balls and hollow plastic spheres) to investigate the relative performance of the filler material. Aluminium [31]-[33] and steel [34] sheets have been used as skins in combination with various foams. These studies showed that the properties of the core material obviously is significant, but also proved that the performance can be optimized with a proper choice of material. The foam density is as already stated an important parameter, also for sandwich structures, and some authors have tried to investigate the influence of the foam density in a systematic manner. Rajaneesh et al. [35] studied the bending behaviour of sandwich plates consisting of GFRP skins and PVC cores both theoretically, experimentally and numerically. They stated that the behaviour of the panel is governed by three competing failure modes, defined as core indentation, core shear, and face failure by microbuckling.

It is clear from the literature that a myriad of different polymer foams and skin materials that can be combined to create a sandwich structure is available. In this study, we wanted to experimentally investigate the energy absorbing capability of two different polymeric foams (XPS and EPP) used as core material in a crash component during quasi-static loading. XPS is mainly used as an insulation material, while EPP is typically applied in energy absorbing components. Both the base material and the production method differ significantly between the two foams. Three different densities have been tested for each foam type. To characterize the foams, a large number of compression tests were conducted on specimens loaded in different material directions. Then, quasi-static impact tests on sandwich structures were performed. The sandwich panels consisted of 50 mm thick polymeric foam cores of the different materials, and skins of 0.8 mm thick Docol 600DL steel plates. Components without the front plate were also tested to investigate the effect of covering the foam core. Within the experimental limitations of this study, it seems clear from the presented results that if low weight combined with maximum energy absorption are the primary interests, an XPS foam as core seems to be beneficial, while if force reduction and minimum back-plate displacement are most important, an EPP foam as core seems to be a better choice. Thus, the response of the crash component is

largely determined by the properties of the core material during quasi-static loading. It also seems possible to optimize the protection level of such components by proper design.

2. Materials

2.1 Skin and core materials

The skins of the crash components used in this study are made of 0.8 mm thick plates of the medium-strength, high-hardening, Docol 600DL steel. This steel has been heat treated to obtain a dual-phase microstructure of ductile ferrite and strong martensite, where the martensite content determines the strength of the material. Docol 600DL is much used by the automotive industry for car safety components, and the plates were produced and delivered by Swedish Steel AB (SSAB). Nominal mechanical properties for the direction transverse to the rolling direction are provided by the supplier, and the yield stress is reported to lie between 280 and 360 MPa, while the tensile strength should be between 600 and 700 MPa. Note that steel with a density of 7850 kg/m^3 cannot be defined as a light alloy. Thus, the areal weight of the crash components could have been significantly reduced by selecting skins of a more lightweight material. However, since both the strength and ductility of the selected steel are high compared to most light alloys, such as e.g. aluminium sheets, skins of Docol 600DL were used in this study to avoid fracture in the front and/or back plate of the structure during loading.

Two types of polymeric foam with a nominal thickness of 50 mm and three different densities were considered as core material. The first foam is extruded polystyrene (XPS) from Sundolitt [36]. XPS is a closed-cell foam based on the monomer styrene (C_8H_8) having a typical density range of about 28-45 kg/m^3. It has high relative strength, very low weight, low thermal conductivity, and is mainly utilized as thermal insulation. Continuous foam plates are produced by an extrusion process where molten beads of polystyrene is mixed with a blowing agent and other additives before it is extruded through a flat nozzle which gives the plates their desired profile and thickness. After cooling, the plates are cut into proper lengths. Three different nominal densities of XPS have been investigated here, namely 30, 35 and 45 kg/m^3, which are called XPS-250, XPS-400 and XPS-700, respectively. The digits in the names indicate the plateau stress (or compressive strength) in kPa of the material. The XPS foams were delivered as plates with nominal dimensions 1185 mm × 585 mm × 50 mm. Nominal mechanical properties of XPS are listed in Table 1, while Figure 1a) shows a SEM image of the cell structure in XPS-400. The cell structure was found to be similar for XPS-250 and XPS-700. It should be

mentioned that XPS in general is flammable. For this reason, not all XPS products are suitable in structural applications, but it is possible to add flame-retardants to the foam so that fire requirements are met. The fire safety of XPS is not addressed any further in the following, since the main objective of this study is to reveal the mechanical response and energy absorbing capability of the foams.

The second core material is expanded polypropylene (EPP) from ARPRO [37]. EPP is an addition thermoplastic polymer made from the monomer propylene (C_3H_6) with a density range from 20 to 200 kg/m^3. EPP has many of the same beneficial properties as XPS, but in contrast to XPS, which is rather friable and may fracture upon loading, EPP foams are known to absorb energy without failure. Thus, EPP is often used in safety components related to crashworthiness by the automotive industry (such as interior crash pads for head/knee protection and bumper cores). EPP consists of pellets produced by a foamed polypropylene. After various pre-treatments, the foam is produced by steam chest moulding of the pellets, using either a crack-fill or a pressure-fill process. For the highest densities, no post-treatment after moulding is required, but for the lowest densities post-treatment in an oven is recommended. Three different types of EPP have been applied in this study: EPP-5122, EPP-5130 and EPP-5170 with nominal densities of 30, 50 and 100 kg/m^3, respectively. Here the two last digits in the name indicate the bulk density (in kg/m^3) of the beads. Nominal mechanical properties of EPP are listed and compared with XPS in Table 1, while Figure 1b) shows a SEM image of the microstructure of EPP-5130. As seen, the microstructures of XPS-400 and EPP-5130 are similar, but the cell size seems somewhat smaller for the latter. The EPP foam with the lowest density (30 kg/m^3) was delivered as plates cut from a block of material with nominal dimensions 1200 mm × 800 mm × 180 mm, while the two other EPP foams were delivered as plates with nominal dimensions 2000 mm × 1000 mm × 50 mm.

2.2 Experimental setup for material tests

Holmen et al. [38] conducted uniaxial tensile tests on standard dog-bone specimens (see Gruben et al. [39] for the geometry) taken from the same 0.8 mm thick plates of Docol 600DL as used herein to determine the behaviour of the material. In the quasi-static setup, triplicate tests were done in three different in-plane directions ($0°, 45°, 90°$) with respect to the rolling direction of the plate. The crosshead velocity of the uniaxial test machine was 2.0 mm/min in all tests, giving an initial strain rate of approximately 5×10^{-4} s^{-1} in the gauge area of the

specimen. During testing, the force was measured by a calibrated load cell, while the displacement of the specimen was measured by both an extensometer and 2D-DIC.

Uniaxial compression tests of the polymer foams were performed under displacement control in an Instron universal testing machine. Cubic specimens with edge lengths of 50 mm were cut from the centre of the as-received plates to avoid possible edge effects. Two different sample geometries were initially investigated: 50 mm cubes and cylinders with diameter and height equal to 50 mm. Since the difference in mechanical response between the two geometries was found to be small, it was chosen to use cubes in the rest of the study to simplify both the sample preparation and the DIC measurements.

A large number of material tests were then carried out in two test series to characterize the quasi-static mechanical response of the different foams. In Series 1, the anisotropy of the foams was revealed by conducting compression tests on cubes loaded in the thickness (or normal) direction (ND), the longitudinal direction (LD), and the transverse direction (TD) of the plates. In Series 2, the inherent surface layers due to the production process of the foams were removed to check if this affected the overall mechanical response of the material. This was only investigated for XPS-400 and EPP-5170, but in all three loading directions. All tests were repeated 5 times, and the crosshead velocity of the test machine was 3.0 mm/min in these tests, giving an initial strain rate of 1×10^{-3} s^{-1}. The complete test matrix for the foam compression tests is given in Table 1.

Prior to testing, each sample was given an identification number before being carefully measured and weighed. Based on these measurements, the density as given in Table 2 was determined. During testing, the specimens were compressed between two hardened steel platens. The load P was registered with a calibrated load cell, while the vertical displacement w was measured both by the stroke of the test machine and edge tracing of the rigid platens using a predefined vector in the finite element based DIC-code eCorr v4.0 [40]. Based on these measurements, the engineering stress s and the engineering strain e were calculated as

$$s = \frac{P}{A_0}, \qquad e = \frac{w}{h_0} \tag{1}$$

where A_0 is the initial cross-section area and h_0 is the initial height of the specimen. Assuming a negligible Poisson's ratio for the foams, i.e., $A_0 \approx A$, the Cauchy (true) stress σ and the logarithmic (true) strain ε can be found through the relations

$$\sigma = \frac{P}{A} = \frac{P}{A_0}, \qquad \varepsilon = \ln\left(e+1\right) \tag{2}$$

All tests were automatically stopped when the load reached approximately 5 kN. Pictures for both local and global 2D-DIC analyses were provided by a Prosilica GC2450 camera equipped with a 50 mm Nikon lens and synchronized with the load measurements. The image resolution during testing was 2448×2050 at 8-bit pixel depth, while the frame rate was 0.5 Hz at this strain rate. Data were logged with a frequency of 10 Hz. A fine-graded speckle pattern was also applied to the foam samples before testing to obtain an increased contrast for the displacement- and strain-field measurements.

2.3 Experimental results

Results from the tensile tests on the 0.8 mm thick Docol 600DL steel skins are plotted in Figure 2 in terms of a) force-elongation curves and b) true stress-plastic strain curves until necking in the different material directions. Here, the strains until necking were obtained using a virtual extensometer (vector) with an initial length of 40 mm in the DIC software eCorr [40]. As seen, the skin material can be considered as both isotropic and ductile with a small variation in elongation to failure.

Figure 3 shows pictures of typical foam samples before and directly after testing. It is worth noting that all samples showed viscoelastic behaviour and recovery when unloaded. The degree of recovery was estimated based on height measurements of the sample immediately, one day, and one week after the tests. The general trends were that the recovery increased with increasing level of compaction and foam density. The recovery was also found to be stronger for EPP foams than for XPS foams.

Figure 4 and Figure 5 show respectively the true stress-strain curves from all tests of the XPS and EPP foams loaded in different directions, while Figure 6 compares the stress-strain response in ND for the two foam types with different densities. All samples showed typical closed-cell foam behaviour, i.e., a linear elastic region, a plateau region with large plastic strains, and finally a densification region where the cells become compacted. Mean values of density ρ, elastic modulus E, yield stress σ_y, plateau stress σ_p and densification strain ε_D for the tests in ND at a strain rate of 1×10^{-3} s^{-1} are given in Table 2. Here, E is calculated from the linear elastic region of the stress-strain curve, σ_p is taken as the mean stress in the interval

between 0.2 and 0.4 compressive strain, while σ_y and ε_D are obtained by a best fit to a crushable foam model from the literature (see Reyes et al. [41] for details).

From the 90 quasi-static compression tests conducted, we can draw some main conclusions. First, the scatter between parallel tests is in general small. The exceptions are the XPS foams with the lowest densities compressed in ND, where a slightly more unstable behaviour is observed. Second, the anisotropy of the foams seems moderate at true strains below 1-1.5, especially for EPP. For XPS with the highest density, a more pronounced effect of material direction is seen, and a drop in plateau stress is obtained when moving from ND to LD/TD. This drop is opposite for EPP with the highest density. Nonetheless, the foams may all be considered as isotropic for most engineering applications. Third, the elastic modulus, the yield stress and the plateau stress display a distinct increase with foam density, as also confirmed in Table 2. The densification strain for XPS is rather constant and independent of density, while it decreases with increasing density for EPP (see Figure 6). However, the density variation between the EPP foams is larger than for the XPS foams. For the same density, XPS foams are found to be significantly stiffer and stronger than corresponding EPP foams. The material strain-hardens somewhat for all the tested materials, leading to a plateau stress that increases with compressive strain.

Figure 7 shows the effect on the mechanical behaviour by removing the surface layer of the XPS-400 and EPP-5170 foam samples before testing in different directions. If these curves are compared with the corresponding true stress-strain curves in Figure 4 and Figure 5, where the surface layers are still present, negligible differences are seen. Thus, the surface layer does not seem to have any major influence on the global mechanical response of the foams investigated in this study.

Foams are known to have a Poisson's ratio close to zero in the plastic domain [11], [26]. It is also established that when foams are compressed, zones of highly compacted material surrounded by regions with lower strains will form due to the porous structure. As the compression increases, the localised areas extend and propagate outwards [26]. To investigate these effects for the applied foams, some specimens were examined in more detail using the DIC-code eCorr [40]. Displacement- and strain-fields were obtained by a global optimization on a mesh of 16×16 Q4 elements superimposed onto the pictures of the deforming specimens. Typical strain fields of XPS and EPP foams are shown in Figure 8 at a compression of approximately 25 mm in ND. These fields reveal a distinct difference in the deformation mode and strain localization for the two types of foam when crushed, even though the global stress-strain response shown in Figure 4 and Figure 5 looks similar. Both foams display strain

300 localization with negligible elongation in the transverse direction. However, while the strain localization in XPS is seen to start in a sharp band in the middle of the specimen and expand 302 outwards, the strain localization in EPP seems to appear randomly distributed over the height of the sample. This local response may explain why EPP foams strain harden more in the plateau 304 region than XPS foams, and is probably a consequence of the production process. Since XPS foams are extruded, the density will vary over the thickness, and is often found to be lower in 306 the center of the material [42]. EPP foams, on the other hand, are expanded resulting in a more evenly distributed density. It should also be mentioned that the strain localization in the highest 308 density XPS foam occurred in distinct bands closer to the surface layers than in the lower density foams where it took place in the middle. These localized bands are illustrated by the 310 white arrows in Figure 9. From these results, we conclude that local variations occur between different foam types, even though the global stress-strain response is rather similar. It is also 312 safe to assume a negligible Poisson ratio in the plastic domain for all the foams applied.

314 3. Component tests

3.1 Experimental setups

316 Quasi-static impact tests on different target configurations were carried out to reveal the mechanical response. The steel skins were the same in all components, while the core material 318 and density varied. Further, the thickness of the skins and the core was kept constant at 0.8 mm and 50 mm, respectively, whereas the in-plane dimensions were taken as 400 mm × 400 mm in 320 all tests. The target configurations tested were: 1) sandwich structure, i.e., the target consisted of front and back steel skins with the various polymeric foams described in Section 2 as core, 322 2) core and steel plate, i.e., the target was similar to that in configuration 1, but without the front skin and 3) skins only, i.e., the target consisted of one or two steel plates in contact without the 324 core. In the tests, the square components were bolted to a rigid circular frame with an inner span diameter of 300 mm. Clamping was provided by 12 equidistant M12 bolts that fixed the target 326 to the test rig. Each bolt was tightened to 2 Nm using an instrumented torque wrench to avoid damage to the rather soft targets. No clamping ring was used on top of the target plate in any of 328 the tests for the same reason. 3D-DIC was used to measure the out-of-plane deflection of the back skin in all tests. Pictures of the various target configurations in the quasi-static setup are 330 shown in Figure 10. The impactor nose was originally designed to imitate an idealised knee

during a crash situation [43], and was thus found ideal to reveal the energy absorbing capabilities of the various configurations during loading.

The tests were conducted under displacement control in the same Instron universal testing machine equipped with the same load cell as used in the material tests. The loading was stopped at a stroke of 50 mm for the sandwich components, after some fracture in the foam for the tests without the front skin, or at a force of 95 kN for the skins only. The crosshead velocity during testing was also the same as in the quasi-static material tests, i.e., 3 mm/min. The tests were instrumented by three Prosilica GC2450 cameras synchronized with the load measurements at a frame rate of 0.5 Hz. Two of the cameras were used to measure the out-of-plane deflection of the back plate by 3D-DIC, while the last camera was used for point-tracking of the impactor displacement. Camera calibration is required for 3D-DIC in eCorr, and this was done by photographing a cylinder covered by a checkerboard pattern with known geometry before and after testing. After calibration, the standard deviation of the errors in the calculated 3D model was found to be less than a tenth of a millimetre when compared to the exact geometry (see e.g. [44] for details). Prior to testing, the foam cores were measured and weighed to determine the density, and the underside of the back sheets facing the cameras was painted with a black and white speckle pattern for 3D-DIC measurements. In total 20 quasi-static component tests were carried out in this study and the main results are presented below.

3.2 Experimental results

Experimental data in terms of energy absorption versus stroke displacement from the quasi-static tests are given in Table 3 as work W at different levels of striker displacement w. This table also contains the work until the first failure in the foam core for configuration 2, i.e., the component without the front skin. Failure in the foam core was not observed in any of the tests for the sandwich structures in configuration 1, where the foam core was covered by the skin. Note that failure occurred much earlier, i.e., at smaller striker displacements, for XPS than for EPP foams. Parallel tests were carried out for some of the configurations, and the scatter was in general found to be modest (see Table 3). Measured force-displacement curves are plotted in Figure 11, while displacement profiles of the back plate from 3D-DIC measurements at a stroke of 50 mm are given in Figure 12. Pictures of some typical foam cores and skins after testing are shown in Figure 13.

Figure 11a) and b) show that the force level increases monotonically with foam density for the same displacement and core material in both configuration 1 and 2. Furthermore, XPS-700

absorbs the most energy in configuration 1, even though EPP-5170 is more than twice as dense. In general, XPS foams absorb much more energy than EPP foams in this configuration at the same density and displacement. This is related to the higher stiffness and strength of XPS compared to EPP with similar density (see Table 1 and Table 2). In configuration 2, however, XPS fracture long before EPP, and EPP absorbs most energy at large displacements. This is further indicated by the measured out-of-plane displacement profiles shown in Figure 12. These profiles show that large forces result in large displacements of the back skin, and subsequently large energy absorption, during quasi-static loading. While a foam core of XPS-700 results in the largest displacements in configuration 1, EPP-5170 results in the largest displacements in configuration 2. This is also reflected in the force-displacement curves in Figure 11. Figure 13a) shows that fracture in the core is prevented in configuration 1, while Figure 13b) shows that the fracture mode is somewhat different for the two foams in configuration 2. For XPS the fracture grows almost vertically along the sides of the impactor in a rather brittle manner, whereas for EPP the fracture develops more diagonally away from the impactor, spreading the applied force over a larger area of the back skin. Figure 11a) and b) confirm that the sandwich structure in configuration 1 absorbs much more energy than the foam cores without the front skin in configuration 2 for the same displacement. This is probably due to membrane stretching of the front skin and a better load distribution over the core at large strains.

For the skins only, i.e., configuration 3, a rather complex buckling process takes place in the sheets already at moderate deformations as seen in Figure 11c) and Figure 13c), and the load is mainly carried by membrane stretching as the displacement increases. The out-of-plane displacement profiles (not shown for brevity) takes the form of the impactor, so it is clear that the nose-shape of the striker strongly influences these results. At a displacement of around 40 mm, the single skin started to fail at the support and the force drops. Such failure was not observed for the double skins, but the boltholes were clearly elongated (see Figure 13c)). From the 3D-DIC measurements, the calculated strain fields confirmed that the strains in the centre of the back plate are small (typically less than 5%), but significantly higher (more than 50%) at the boundary. The buckling of the steel sheets around the rim could have been better controlled by a fully clamped boundary, but such boundary conditions are unlikely for an energy absorber in a car-crash situation. In that sense, the applied boundary conditions are more realistic.

Figure 11d) compares the energy absorption in some of the configurations. The work increases rapidly at large deformations, meaning that the loading is mainly carried by membrane stretching in the skins when the foam core becomes sufficiently compressed. Without the foam core, this increase in force takes place at a much lower displacement.

4. Discussion

In order to design an optimal component for energy absorption, at least four different premises are important. These are: 1) low total weight, 2) reduced force transmission to the underlying structure, 3) high total energy absorption and 4) low out-of-plane displacement of the back skin. In addition, complete failure of the whole component could obviously be catastrophic, but since none of the configurations investigated in this study failed at critical points, this is left for further studies. From the data of the component tests given in Figure 11 and Table 3, one can see that when the density of the foam increases, both the force level and the energy absorption increases for the same striker displacement. This seems valid independent of foam type and target configuration, and is further illustrated in Figure 14 where the force and energy absorption are plotted as a function of foam density at a striker displacement of 50 mm. From these plots, it is also seen that XPS foams experience higher forces and energy absorption than EPP foams for the same density in both configuration 1 and 2. Thus, if energy absorption is the primary interest, XPS foams seem to be beneficial, but if force reduction is most important, EPP foams seem to be a better choice. This is related to the fact that XPS is significantly stronger and stiffer than EPP with corresponding density (see e.g. Table 2).

Another important response parameter is the out-of-plane displacement w_b of the back skin, and Figure 12 shows that this value decreases for decreasing density under quasi-static loading conditions. The obvious reason is that a foam core with a low density is more easily compressed. This trend is similar in configuration 1 and 2, but the back-plate displacements are noticeably lower in configuration 2 than in configuration 1 due to an increased compaction of the unprotected core. Furthermore, EPP cores cause lower back-plate displacements than XPS cores in configuration 1, probably because EPP is weaker and less stiff than XPS, while in configuration 2 they are rather similar. From these results, it may be argued that a low-density EPP foam should be chosen as core material if back-plate deflection is the main design criterion.

It is also interesting to compare the quasi-static response of the component with and without the front skin. In this study, the weight of one steel skin is about 1 kg, while the weight of the foam core varies between 0.24 kg and 0.80 kg depending on the density. Thus, the skins represent 70-90% of the total weight of the component. If the front plate is removed or replaced by a lighter material, the total weight of the component can be much reduced. Figure 12 and 14 show that the back-plate displacement, the force and the energy absorption are in general much lower for components without the front skin. Thus, components in configuration 2 are superior to those in configuration 1 in terms of weight, force reduction and back-plate displacement, but

the energy absorption is significantly reduced. Based on this, one may speculate if a weaker and lighter front skin material could increase the energy absorption, while at the same time maintaining the beneficial effects seen in configuration 2. As long as the back skin is strong enough to carry the loading without failure, it is anticipated that the front skin can be replaced by another material. However, in order to confirm this, additional studies are required.

The mechanical response of foams with similar densities is considered next. Under such conditions, the mass of the component will be the same, so the possible difference in response is only due to the core material. In this study, XPS-700 and EPP-5130 have practically identical densities, while the density of XPS-250 is approximately 10% higher than that of EPP-5122. It is seen that in terms of energy absorption, XPS outperform EPP for the components both with and without the front skin (Figure 14 b)). However, the force level in XPS is higher than in EPP for similar densities (Figure 14 a)), and EPP gives in general lower back-plate displacements than XPS (Figure 12). These results are again linked to the fact that the stiffness and strength of XPS foams are significantly higher than for corresponding EPP foams (Table 2). However, for components in configuration 2, the low-density foams give comparable energy absorption, force level and back-plate displacement.

It is customary to specify the efficiency of energy absorbers in terms of their specific work W_s [45]. In the following, this is defined as the total work W_t at a given striker displacement (see Table 3) divided by the total mass m_t of the component, i.e.,

$$W_s = \frac{W_t}{m_t} \tag{3}$$

Here, m_t varies from a minimum of 1.24 kg using EPP-5122 in configuration 2 to a maximum of 2.80 kg using EPP-5170 in configuration 1. The specific work for a striker displacement of 50 mm is plotted versus foam density in Figure 15 a). It is seen that the overall response is similar to the absolute values given in Figure 14 b), and that XPS in configuration 1 outperforms the other configurations also with respect to the specific energy absorption. However, the specific energy of the components without front skin are closer to those with front skin (which is natural as the weight is lower). Note also that the specific energy absorption for the unprotected XPS-700 core in configuration 2 becomes higher than the protected EPP-5130 core in configuration 1. This could not be seen from Figure 14 b).

As an alternative, Mohotti et al. [46] introduced an energy efficiency parameter E_d for plates subjected to low velocity impacts. This parameter allows comparing results in terms of total energy absorption per unit maximum back-plate displacement. As we are investigating the quasi-static behaviour in this study, we have used the following definition

$$E_d = \frac{W_t}{w_b} \tag{4}$$

where W_t is as before the absorbed energy at a given striker displacement and w_b is the maximum back-plate displacement measured by 3D-DIC. The energy efficiency parameter for a striker displacement of 50 mm versus the foam density is shown in Figure 15 b). No major difference in the trends is seen between Figure 15 a) and b), and the results indicate that XPS in configuration 1 outperforms the other configurations also with respect to energy efficiency. However, since the influence of the back-plate displacement is included in E_d, EPP approaches XPS in configuration 1 for the lowest-density foams.

It is difficult to make strict conclusions based on the results presented above, but it seems apparent that the total weight, the transmitted force, the energy absorption and the out-of-plane displacement of the back skin of the component all depend on the core material. Within the experimental limitations of this study, it seems clear that if low weight combined with maximum energy absorption are the primary interests, an XPS foam is beneficial as core material, while if force reduction and minimum back-plate displacement are most important, an EPP core may be a better choice. Thus, the response of the component is largely determined by the properties of the core material during quasi-static loading. It also seems possible to optimize the protection level of such components by proper design. Since both XPS and EPP seem to have advantages and disadvantages with respect to the studied response parameters, a functionally graded foam with layers of XPS and EPP having different densities may be favourable. Such functionally graded foams have been found to be superior compared to uniform foams, and have received some attention in the literature [14]-[15]. However, such an optimization requires numerical simulations, which is outside the scope of this study.

5. Conclusions

In this study, we have experimentally investigated the quasi-static energy absorbing capability of two different polymeric foams (XPS and EPP) with varying density used as core material in a crash component. In addition to a number of material tests, quasi-static impact tests were performed on three different target configurations. The following main conclusions can be drawn based on the obtained results:

- From the 120 compression tests carried out on square foam samples, the scatter between parallel tests was found to be small. Some anisotropy between different loading directions was observed, especially for the XPS foams, but the foams may be considered as rather isotropic. As expected, the elastic modulus, the yield stress and the plateau stress increased significantly with foam density, while the inherent surface layers on the various foams did not affect the overall mechanical response of the materials much. However, XPS foams were found to be much stiffer and stronger than EPP foams with corresponding density. Both foam types revealed viscoelastic behaviour. Finally, based on DIC measurements the strain localization was found to be very different between the foam types even though the global mechanical response was similar.
- From the 20 quasi-static impact tests, it was observed that the force level and the energy absorption increased monotonically with foam density both for the covered and uncovered components. It was also established that XPS foams absorbed considerably more energy than EPP foams with the same density at the same displacement. When the foams were unprotected, they failed in some shear fracture mode, and the rather brittle XPS foams failed before the EPP foams. For the skins only, a rather complex buckling mode took place. At large displacements, the force increased rapidly, indicating that the loading was carried by membrane stretching in the metal skins.
- The components without the front skin were superior to the sandwich components in terms of most response parameters, but the energy absorption was significantly reduced. However, this may be improved by using a weaker and lighter front skin material as long as the back skin is strong enough to carry the loading without failure.
- Within the experimental limitations of this study, it seems clear that if low weight combined with maximum energy absorption are the primary interests, XPS are beneficial as core material, while if force reduction and minimum back-plate displacement are most critical, EPP as core may be a better choice. Consequently, it is not obvious which combination of

the different variables that will gives the best crash component during quasi-static loading. It should however be possible to find an optimized energy absorber by proper design.

A natural continuation of the presented research is to extend the experimental database with dynamic tests and to use the experimental results to calibrate and validate numerical models for finite element simulations of the crash components. To do so, efficient and accurate material models for the polymeric foams are required. It should then be possible to maximise the energy absorption in the component, and at the same time minimise the weight, the transmitted force and the back-plate displacement, by an optimization tool. That is left for future studies.

Acknowledgement

The present work has been carried out with financial support from Centre of Advanced Structural Analysis (CASA), Centre for Research-based Innovation, at the Norwegian University of Science and Technology (NTNU) and the Research Council of Norway through project no. 237885 (CASA). The authors would like to acknowledge Dr. Egil Fagerholt, Mr. Trond Auestad, Mr. Bjarki Sigurdsson, Mr. Asle Tomstad, Mr. Sindre Berdal, and Mr. Lars Einar Bjørgo for assistance with the various experimental programs.

References

[1] M. Paulino, F. Teixeira-Dias, An energy absorption performance index for cellular materials – development of a side-impact cork padding, Int. J. Crashworthiness 16 (2011) 135-153.

[2] D. Wang, S. Zhang, C. Wang, C. Zhang, Structure-material-performance integration lightweight optimisation design for frontal bumper system, Int. J. Crashworthiness 23 (2018) 311-327.

[3] J. Mackerle, Finite element analyses of sandwich structures: A bibliography (1980-2001), Eng. Computation. 19 (2002) 206-245.

[4] M. Avalle, G. Belingardi, A. Ibba, Mechanical models of cellular solids: Parameters identification from experimental tests, Int. J. Impact Eng. 34 (2007) 3-27.

[5] S. Murata, S. Shioya, B. Suffis, Expanded Polypropylene (EPP) - A Global Solution for Pedestrian Safety Bumper Systems. SAE 2004 World Congress & Exhibition, 2004.

[6] G. Slik, G. Vogel, V. Chawda, Material Model Validation of a High Efficient Energy Absorbing Foam. 5th LS-DYNA Forum, Ulm, 2006.

[7] D. Karagiozova, G.S. Langdon, G.N. Nurick, Blast attenuation in Cymat foam core sacrificial claddings, Int. J. Mech. Sci. 52 (2010) 758-776.

[8] M. Avalle, G. Belingardi, R. Montanini, Characterization of polymeric structural foams under compressive impact loading by means of energy-absorption diagram, Int. J. Impact Eng. 25 (2001) 455-472.

[9] L. Cui, S. Kiernan, M.D. Gilchrist, Designing the energy absorption capacity of functionally graded foam materials, Mater. Sci. Eng. A 507 (2009) 215-225.

[10] S. Ryan, T. Hedman, E.L. Christiansen, Honeycomb vs. foam: Evaluating potential upgrades to ISS module shielding, Acta Astronaut. 67 (2010) 818-825.

[11] L.J. Gibson, M.F. Ashby, Cellular solids: Structure and properties, 2nd edition, Cambridge University Press, 2014.

[12] D.S. Cronin, S. Ouellet, Low density polyethylene, expanded polystyrene and expanded polypropylene: Strain rate and size effects on mechanical properties, Polym. Test. 53 (2016) 40-50.

[13] Q.M. Li, I. Magkiriadis, J.J. Harrigan, Compressive Strain at the Onset of Densification of Cellular Solids, J. Cell. Plast. 42 (2006) 371-392.

[14] H. Zhou, Y. Wang, X. Wang, Z. Zhao, G. Ma, Energy absorption of graded foam subjected to blast: A theoretical approach, Mater. Design 84 (2015) 351-358.

[15] B. Koohbor, A. Kidane, Design optimization of continuously and discretely graded foam materials for efficient energy absorption, Mater. Design 102 (2016) 151-161.

[16] J. Zhang, N. Kikuchi, V. Li, A. Yee, G. Nusholtz, Constitutive modeling of polymeric foam material subjected to dynamic crash loading, Int. J. Impact Eng. 21 (1998) 369-386.

[17] Y. Sun, Q.M. Li, Dynamic compressive behaviour of cellular materials: A review of phenomenon, mechanism and modelling, Int. J. Impact Eng. 112 (2018) 74-115.

[18] N.J. Mills, A. Gilchrist, Shear and compressive impact of polypropylene bead foam, Cellul. Polym. 18 (1999) 157-174.

[19] P. Viot, D. Bernard, E. Plougonven, Polymeric foam deformation under dynamic loading by the use of the microtomographic technique, J. Mater. Sci. 42 (2007) 7202-7213.

[20] P. Viot, E. Plougonven, D. Bernard, Microtomography on polypropylene foam under dynamic loading: 3D analysis of bead morphology evolution, Compos. Part A Appl. Sci. Manuf. 39 (2008) 1266-1281.

[21] R. Bouix, P. Viot, J.L. Lataillade, Polypropylene foam behaviour under dynamic loadings: Strain rate, density and microstructure effects, Int. J. Impact Eng. 36 (2009) 329-342.

[22] L. Maheo, P. Viot, Impact on multi-layered polypropylene foams, Int. J. Impact Eng. 53 (2013) 84-93.

[23] L. Maheo, S. Guérard, G. Rio, A. Donnard, P. Viot, Multiaxial behavior of foams-Experiments and modeling, EPJ Web of Conferences 94 (2015).

[24] E. Sadek, N.A. Fouad, Finite element modeling of compression behavior of extruded polystyrene foam using X-ray tomography, J. Cell. Plast. 49 (2013) 161-191.

[25] J. Miltz, O. Ramon, Energy absorption characteristics of polymeric foams used as cushioning materials, Polymer Eng. & Sci., 30 (1990) 129-133.

[26] N. Mills, Polymer Foams Handbook, Butterworth-Heinemann, Oxford, 2007.

[27] S.C.K. Yuen, G.N. Nurick, M.D. Theobald, G.S. Langdon, Sandwich panels subjected to blast loading, in: Dynamic Failure of Materials and Structures, in:A. Shukla et al. (eds.), Dynamic Failure of Materials and Structures, Springer, 2010, pp. 297-325.

[28] K.R. Ramakrishnan, K. Shankar, P. Viot, S. Guerard, A comparative study of the impact properties of sandwich materials with different cores. EPJ Web of Conferences 26 (2012).

[29] J.R. Correia, M. Garrido, J.A. Gonilha, F.A. Branco, L.G. Reis, GFRP sandwich panels with PU foam and PP honeycomb cores for civil Eng. structural applications: Effects of introducing strengthening ribs, Int. J. Struct. Integrity 3 (2012) 127-147.

[30] Y. Zhang, Z. Zong, Q. Liu, J. Ma, Y. Wu, Q. Li, Static and dynamic crushing responses of CFRP sandwich panels filled with different reinforced materials, Mater. Design 117 (2017) 396-408.

[31] S. Avachat, M. Zhou, Compressive response of sandwich plates to water-based impulsive loading, Int. J. of Impact Eng. 93 (2016) 196-210.

[32] W. Huang, W. Zhang, N. Ye, Y. Gao, P. Ren, Dynamic response and failure of PVC foam core metallic sandwich subjected to underwater impulsive loading, Compos. Part B Eng. 97 (2016) 226-238.

[33] N. Ye, W. Zhang, D. Li, W. Huang, W. Xie, X. Huang, X. Jiang, Dynamic response and failure of sandwich plates with PVC foam core subjected to impulsive loading, Int. J. Impact Eng. 109 (2017) 121-130.

[34] I. Karen, M. Yazici, A. Shukla, Designing foam filled sandwich panels for blast mitigation using a hybrid evolutionary optimization algorithm, Compos. Struct. 158 (2016) 72-82.

[35] A. Rajaneesh, I. Sridhar, S. Rajendran, Failure mode maps for circular composite sandwich plates under bending, Int. J. Mech. Sci. 83 (2014) 184-195.

[36] http://www.sundegroup.com/ [Cited: 18.06.18].

[37] http://www.arpro.com/ [Cited: 18.06.18].

[38] J.K. Holmen, O.S. Hopperstad, T. Børvik, Low-velocity impact on multi-layered dual-phase steel plates, Int. J. Impact Eng. 78 (2015) 161-177.

[39] G. Gruben, E. Fagerholt, O.S. Hopperstad, T. Børvik, Fracture characteristics of a cold-rolled dual-phase steel, Eur. J. Mech. A Solid. 30 (2011) 204-218.

[40] https://www.ntnu.edu/kt/ecorr [Cited: 18.06.18]

[41] A. Reyes, O.S. Hopperstad, T. Berstad, A.G. Hanssen, M. Langseth, Constitutive modeling of aluminum foam including fracture and statistical variation of density, Eur. J. Mech. A Solid. 22 (2003) 815-835.

[42] J.P. Hegdal, T.R. Tofteberg, T. Schjelderup, E.L. Hinrichsen, F. Grytten, A. Echtermeyer, Thermal conductivity of anisotropic, inhomogeneous high-density foam calculated from three-dimensional reconstruction of microtome images, J. Appl. Polymer Sci. 130 (2013) 1020-1028.

[43] J.F. Berntsen, Impact loading on parts made of injection-moulded PP. Master's thesis, Norwegian University of Science and Technology, Trondheim, Norway, 2015.

[44] V. Aune, E. Fagerholt, M. Langseth, T. Børvik, A shock tube facility to generate blast loading on structures, Int. J. Prot. Struct. 7 (2016) 340-366.

[45] N. Jones, Structural Impact. Cambridge University Press, Cambridge, 1989.

[46] D. Mohotti, T. Ngo, S.N. Raman, M. Ali, P. Mendis, Plastic deformation of polyurea coated composite aluminium plates subjected to low velocity impact, Mater. Design 56 (2014) 696-713.

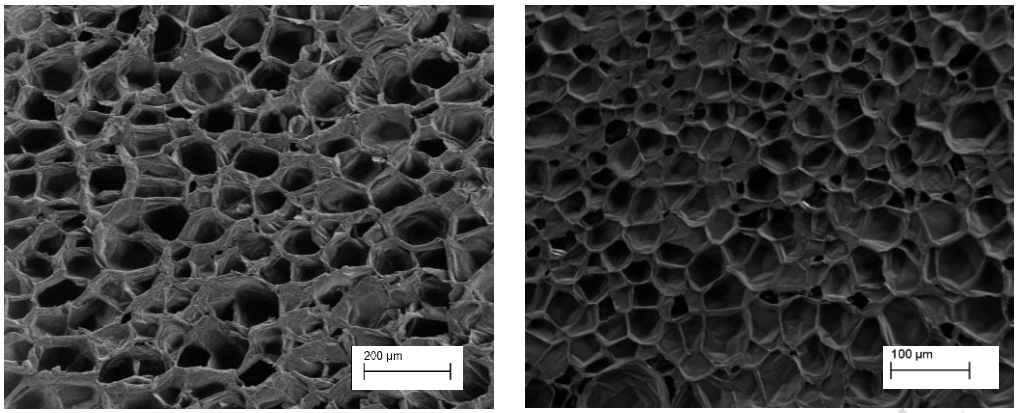

a) b)

Figure 1. SEM images showing the microstructure in a) XPS-400 (ρ = 35 kg/mm^3) and b) EPP-5130 (ρ = 50 kg/mm^3).

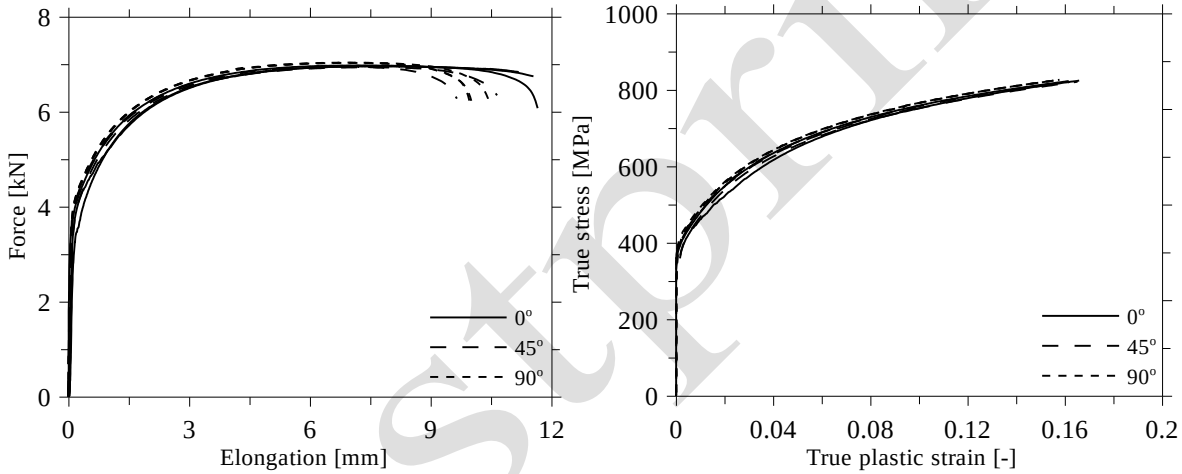

a) b)

Figure 2. a) Force-elongation curves based on DIC-measurements and b) true stress - plastic strain curves until necking using a virtual extensometer of 40 mm from uniaxial tensile tests in three different material directions for Docol 600DL.

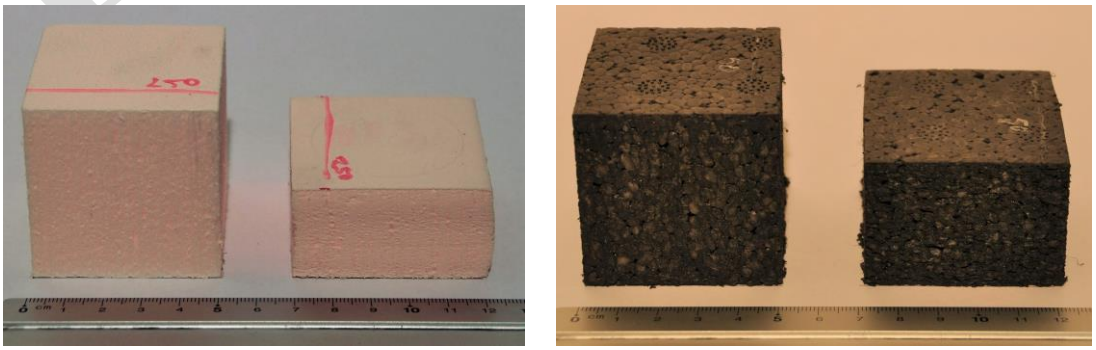

a) XPS-250 b) EPP-5130

Figure 3. Typical foam samples before and after testing.

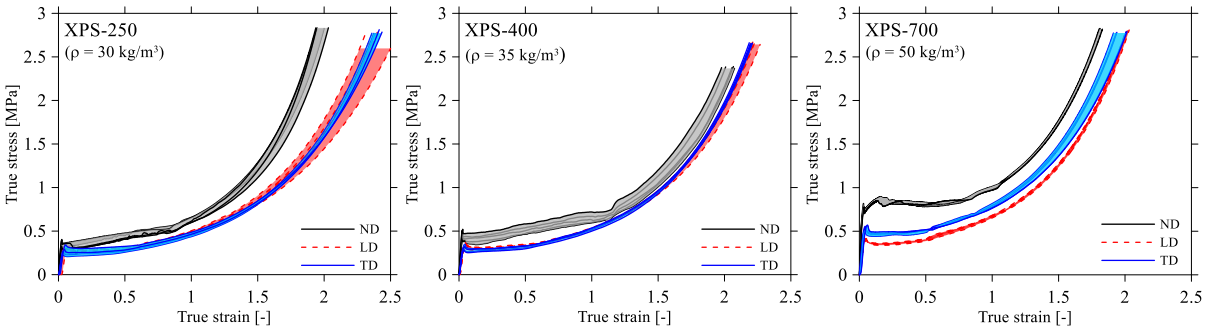

Figure 4. True stress-strain curves for the material compression tests of XPS foams in different directions. The hatched areas illustrate the range of the five parallel tests in each direction.

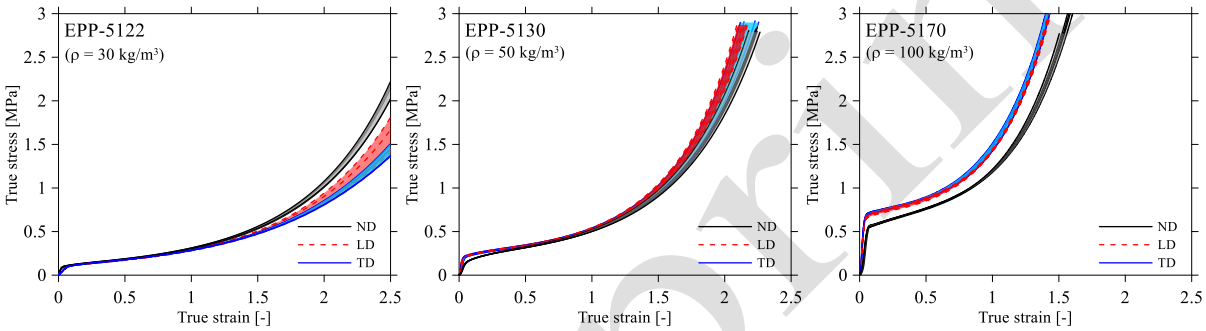

Figure 5. True stress-strain curves for the material compression tests of EPP foams in different directions. The hatched areas illustrate the range of the five parallel tests in each direction.

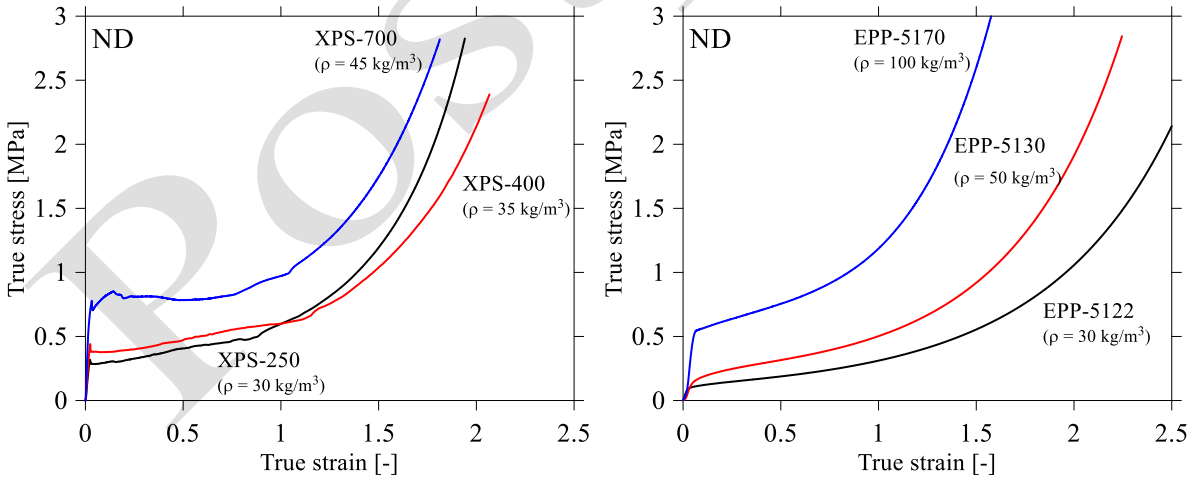

Figure 6. Comparison of true stress-strain curves for XPS (left) and EPP (right) with different densities in ND direction.

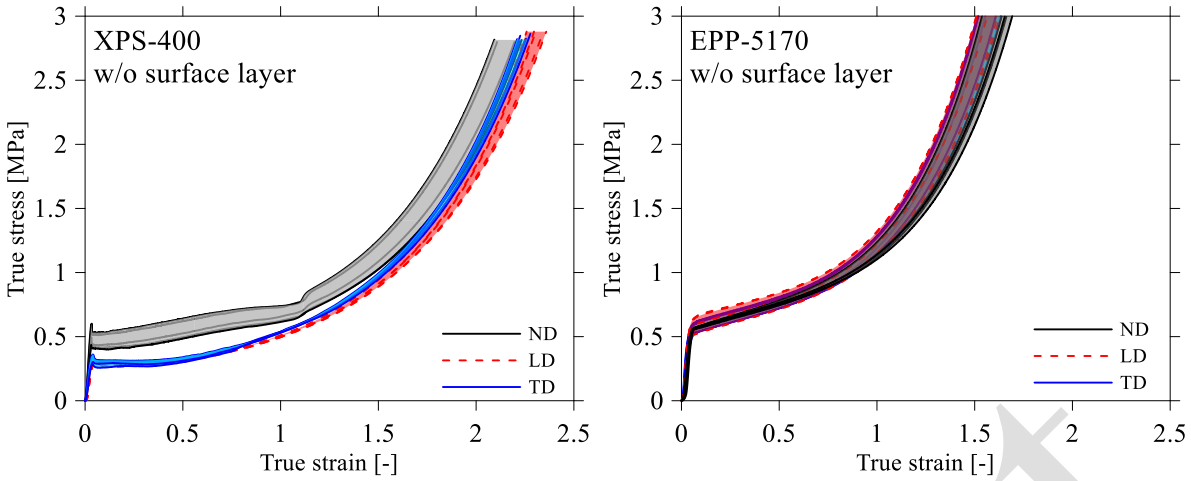

Figure 7. True stress-strain curves from material compression tests of XPS-400 and EPP-5170 in different directions without (w/o) the top and bottom surface layer of the samples. The hatched areas illustrate the range of the five parallel tests in each direction.

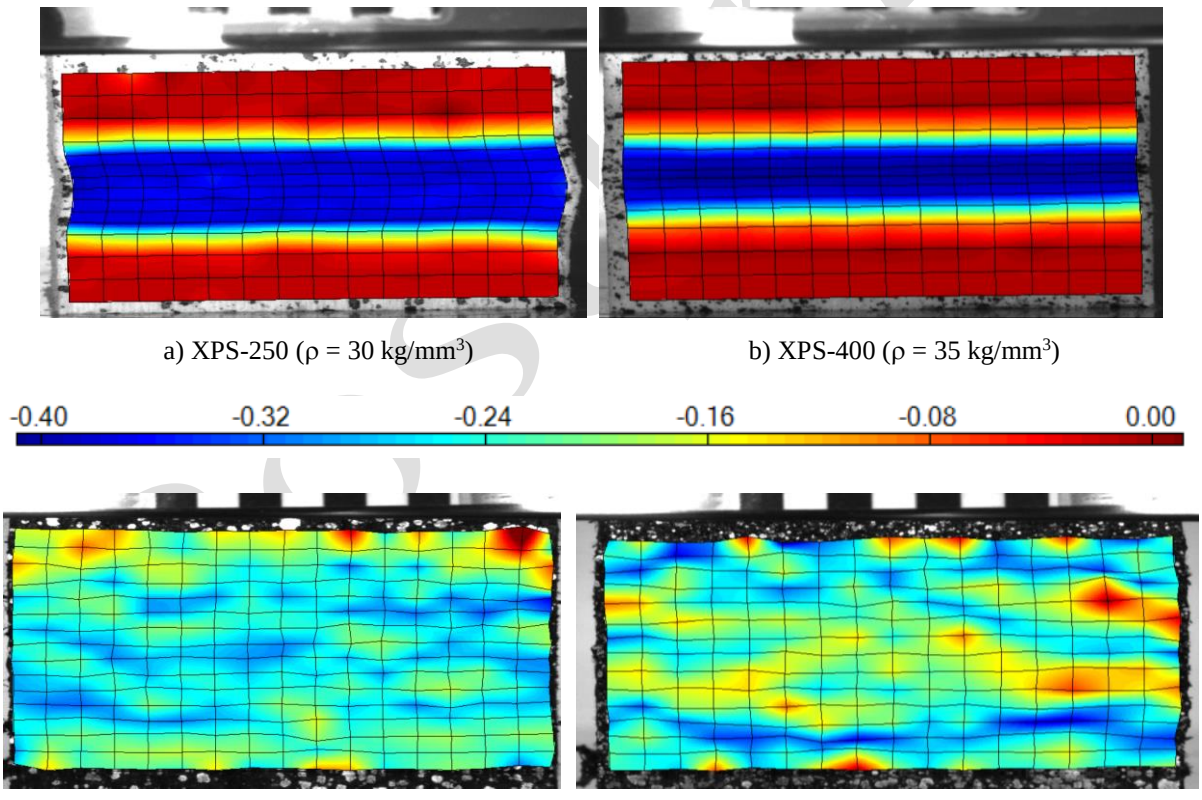

a) XPS-250 (ρ = 30 kg/mm^3) b) XPS-400 (ρ = 35 kg/mm^3)

c) EPP-5130 (ρ = 50 kg/mm^3) d) EPP-5170 (ρ = 100 kg/mm^3)

Figure 8. Measured strain fields from compression tests of a) XPS-250, b) XPS-400, c) EPP-5130 and d) EPP-5170 at a displacement of 25 mm in ND.

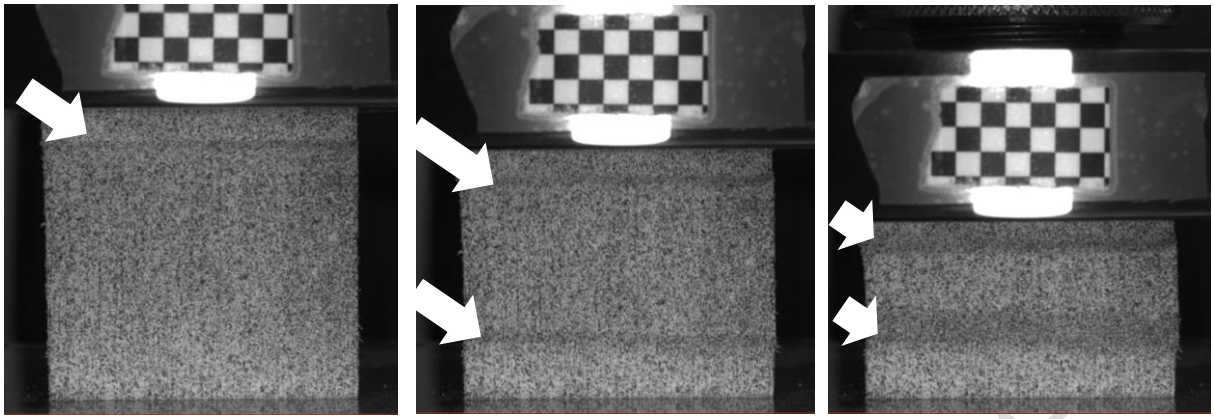

a) $w = 3$ mm b) $w = 10$ mm c) $w = 20$ mm

694 Figure 9. Strain localization in XPS-700 foam during compression at various crosshead displacements (w). The two distinct bands are illustrated by the white arrows.

696

698

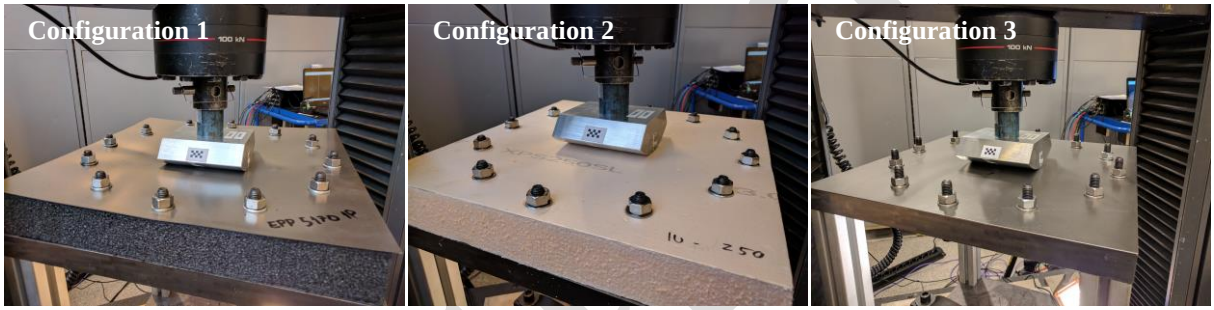

a) b) c)

700 Figure 10. Pictures of the different target configurations used in the quasi-static tests: a) Sandwich structure with foam core (here EPP-5170) and front and back skins in
702 Docol 600 DL, b) component with foam core (here XPS-250) without the front skin, but with back skin in Docol 600DL and c) only skins in Docol 600DL without the
704 foam core.

706

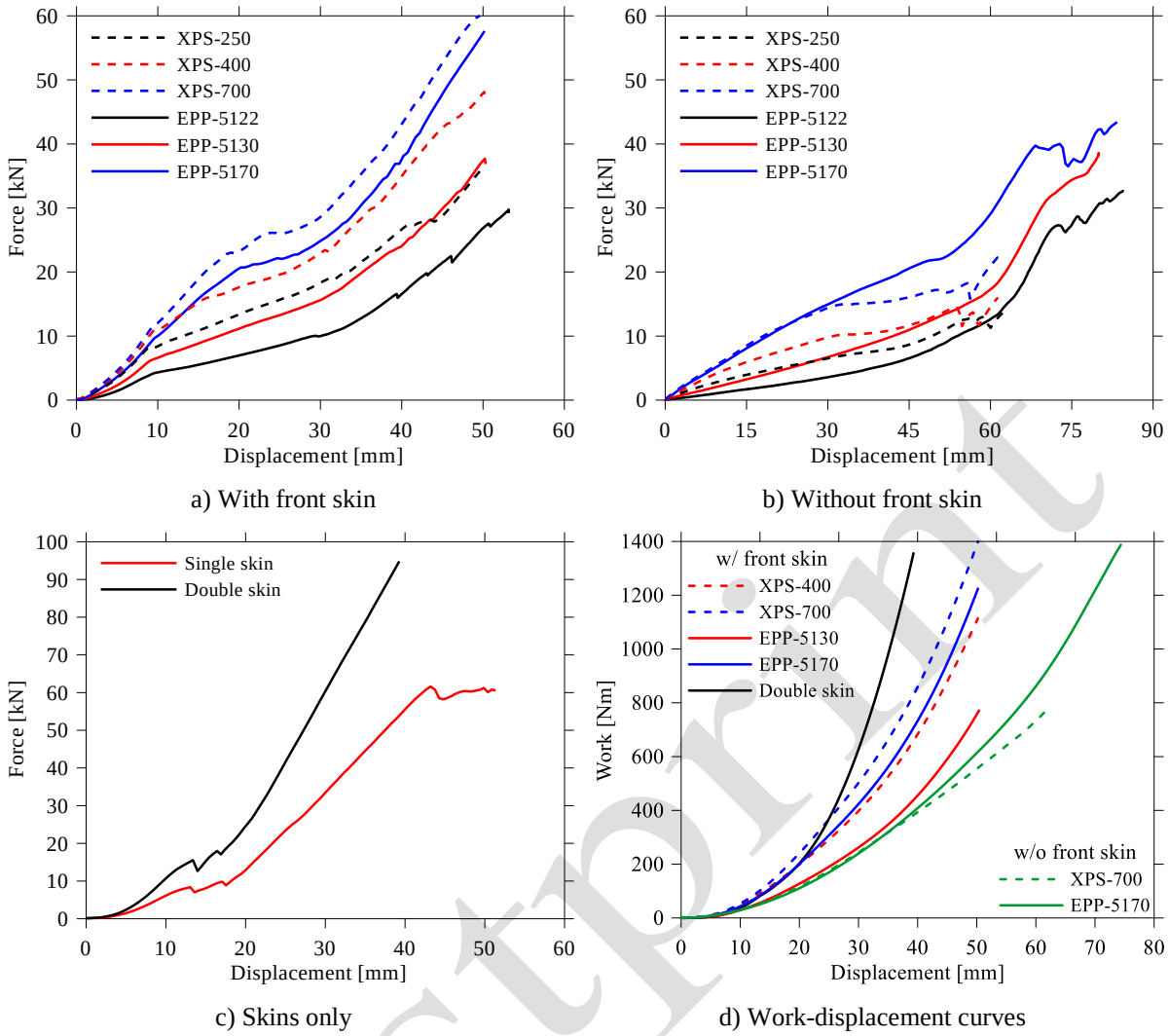

Figure 11. Measured force-displacement curves from quasi-static tests on a) configuration 1, b) configuration 2, c) configuration 3 and d) comparison of energy absorption in typical targets from configuration 1, 2 and 3.

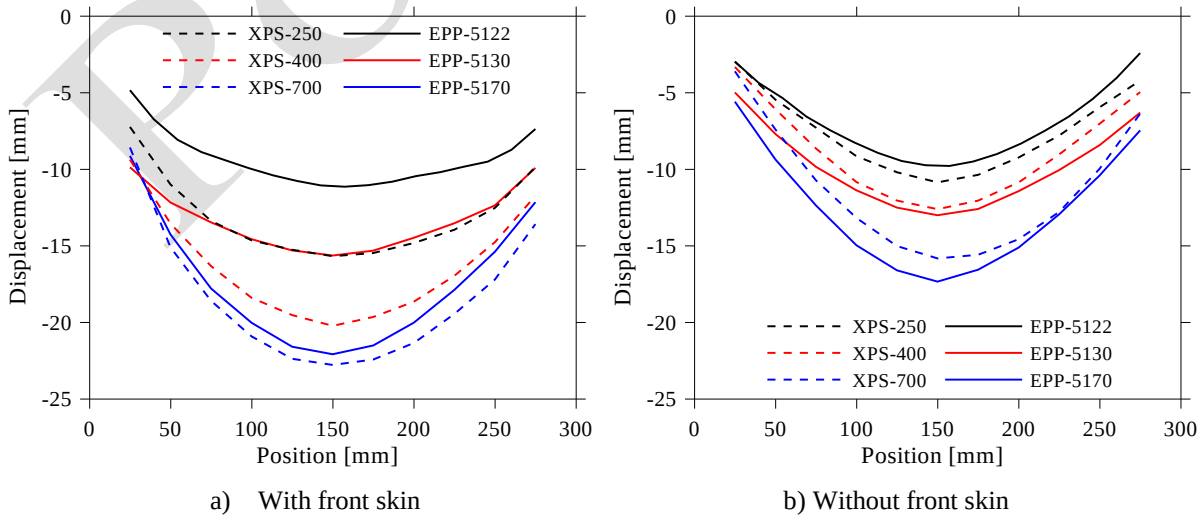

Figure 12. Displacement profiles of the back skin from 3D-DIC measurements at a stroke of 50 mm from quasi-static tests of a) configuration 1 and b) configuration 2.

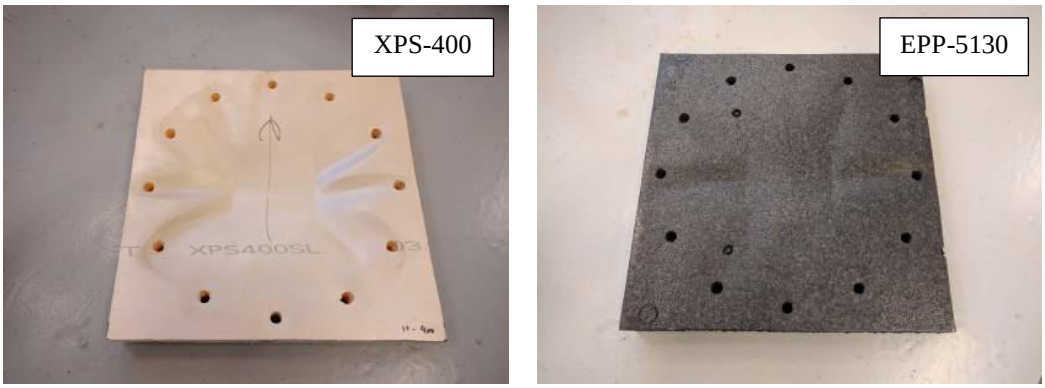

a) With front skin (configuration 1)

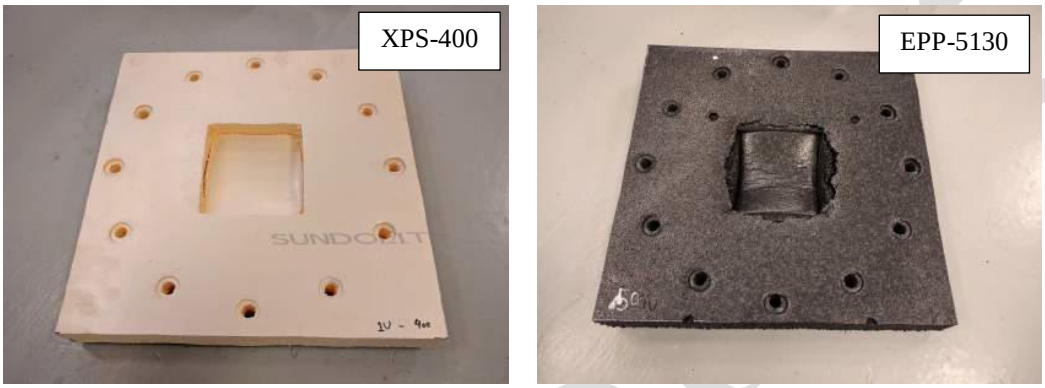

b) Without front skin (configuration 2)

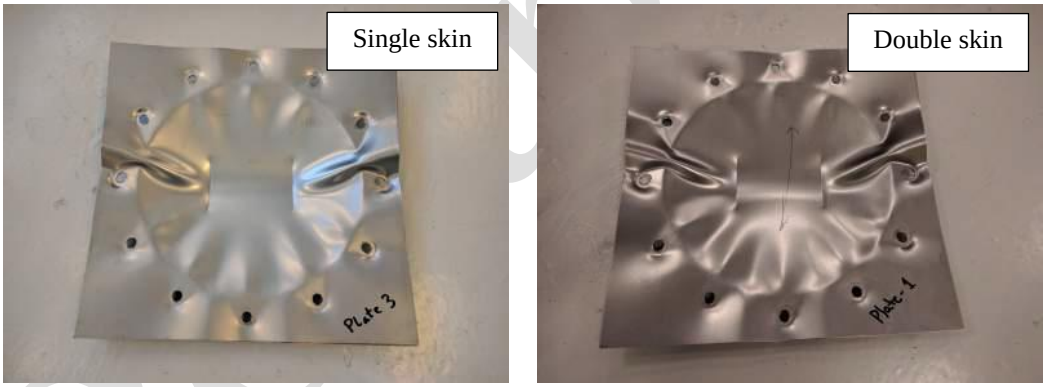

c) Skins only (configuration 3)

Figure 13. Pictures after quasi-static loading of a) the foam cores from configuration 1, b) the foam cores from configuration 2 and c) the skins from configuration 3.

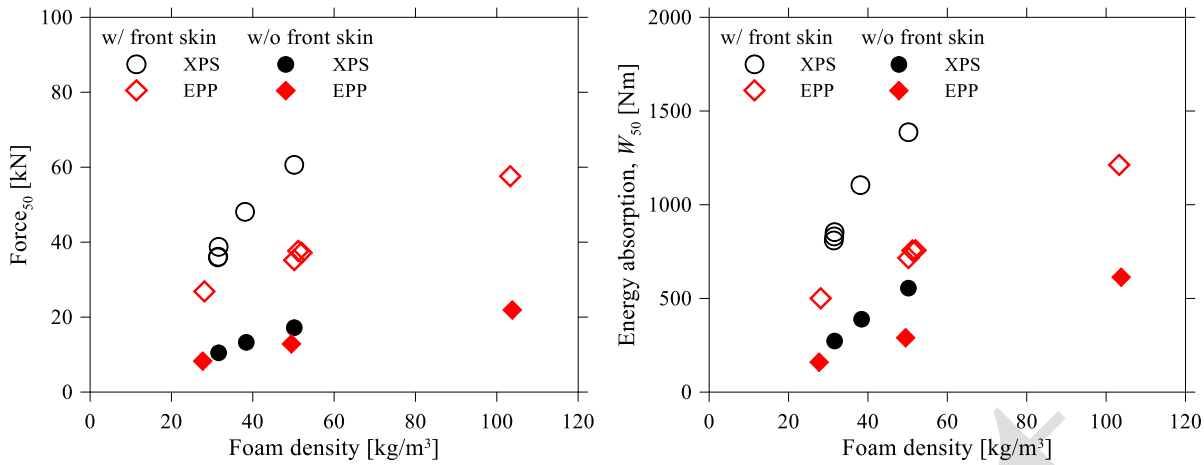

Figure 14. a) Force and b) energy absorption at a stroke of 50 mm versus foam density for configuration 1 and 2. The results from configuration 3 are omitted for clarity.

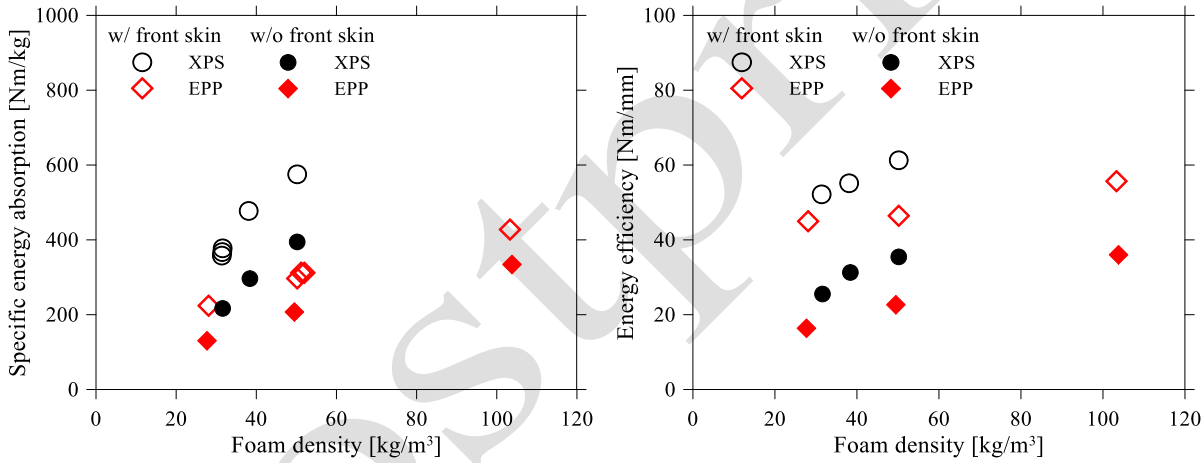

Figure 15. a) Specific work and b) energy efficiency versus density for configuration 1 and 2. The results from configuration 3 are omitted for clarity.

734 Table 1. Nominal material properties and test matrix for material tests.

Material	Name	Nominal properties			Direction	# of samples	
		Density ρ [kg/mm^3]	Elastic modulus E [MPa]	Compressive strength σ_c^* [MPa]		With surface layer	Without surface layer
Extruded polystyrene	XPS-250	30	9.0	0.25	ND	5	-
					LD	5	-
					TD	5	-
	XPS-400	35	15.3	0.40	ND	5	5
					LD	5	5
					TD	5	5
	XPS-700	45	31.0	0.70	ND	5	-
					LD	5	-
					TD	5	-
Expanded polypropylene	EPP-5122	30	2.5	0.15	ND	5	-
					LD	5	-
					TD	5	-
	EPP-5130	50	5.1	0.28	ND	5	-
					LD	5	-
					TD	5	-
	EPP-5170	100	14.3	0.70	ND	5	5
					LD	5	5
					TD	5	5

* At 10% strain for XPS and 25% strain for EPP.

736

738 Table 2. Properties (mean values) of foam samples in ND.

Material	Density ρ [kg/mm^3]		Elastic modulus E [MPa]	Yield stress σ_y [MPa]	Plateau stress σ_p [MPa]	Densification strain ε_D [-]
	Mean	SD				
XPS-250	34.1	0.38	13.7	0.26	0.34	3.36
XPS-400	37.9	0.65	18.5	0.41	0.49	3.68
XPS-700	50.8	0.38	23.5	0.73	0.77	3.46
EPP-5122	29.9	0.52	3.3	0.10	0.16	3.69
EPP-5130	50.7	0.73	5.9	0.19	0.29	2.97
EPP-5170	102.5	1.47	14.5	0.56	0.72	2.65

740

742

Table 3. Data from quasi-static component tests.

Material	Front skin	Measured core height h_{ct} [mm]	Measured density ρ_f [kg/m^3]	Work at different levels of striker displacement $W_{10\text{mm}}$ [Nm]	$W_{20\text{mm}}$ [Nm]	$W_{30\text{mm}}$ [Nm]	$W_{40\text{mm}}$ [Nm]	$W_{50\text{mm}}$ [Nm]	Work until first failure W_f * [Nm]
XPS-250	Yes	51.4	31.4	35.2	141.4	294.6	512.3	809.2	-
	Yes	51.3	31.5	40.2	150.1	307.9	528.0	830.8	-
	Yes	51.4	31.6	44.8	157.2	317.3	540.6	853.7	-
	No	51.3	31.6	16.5	55.7	112.5	184.4	272.5	339.3 (55.5)
XPS-400	Yes	50.4	38.1	49.6	198.3	397.6	683.1	1104.5	-
	No	50.2	38.4	23.7	82.9	168.6	271.2	388.8	431.1 (53.8)
XPS-700	Yes	50.4	50.2	53.6	240.6	502.2	859.1	1386.8	-
	No	50.4	50.2	31.7	116.4	243.6	393.2	554.7	641.1 (55.8)
EPP-5122	Yes	49.7	28.1	17.2	72.3	158.4	288.1	500.4	-
	No	49.9	27.7	5.2	21.7	50.3	93.8	159.9	716.8 (72.5)
EPP-5130	Yes	47.4	50.2	27.1	111.9	239.1	430.4	715.8	-
	Yes	47.7	52.0	29.5	127.3	262.1	455.3	756.7	-
	Yes	48.3	51.2	28.4	117.7	251.6	451.2	755.5	-
	No	48.2	49.5	11.5	44.0	99.2	179.7	290.3	1010.8 (77.5)
EPP-5170	Yes	47.1	103.3	43.0	200.6	423.7	732.9	1212.6	-
	No	47.8	103.8	29.4	110.5	239.4	408.3	613.3	1123.3 (68.4)
Single skin	Yes	1×0.8	7850	21.6	109.8	345.2	794.6	1390.7	-
Double skin	Yes	2×0.8	7850	36.5	196.9	618.0	1413.4	-	-
	Yes	2×0.8	7850	36.3	202.8	627.1	1423.7	-	-
	Yes	2×0.8	7850	34.6	195.0	615.5	1406.4	-	-

744 * Work until first failure in the foam where the numbers in parenthesis give the displacement (in mm) at failure.